Paleoarchean variole-bearing metabasalts from the East Pilbara Terrane formed by hydrous fluid phase exsolution and implications for Archean greenstone belt magmatic processes

David T. Murphy[1]*, Daniel Wiemer[2], Vickie C. Bennett[3], Thomas Spring[1], Jessica Trofimovs[1], Henrietta E. Cathey[1,4]

[1]School of Earth and Atmospheric Sciences, Queensland University of Technology, Brisbane QLD 4000, Australia

[2]School of Earth Sciences, University of Western Australia, Crawley WA 6009, Australia

[3]Research School of Earth Sciences, Australian National University, Canberra ACT 2601, Australia

[4]Central Analytical Research Facility, Queensland University of Technology, Brisbane QLD 4000, Australia

*Correspondence: david.murphy@qut.edu.au

Abstract

Archean greenstone belts contain low grade metamorphic volcanic sequences with localised examples of preserved original volcanic textures and relict magmatic minerals, which are invaluable for inferring volcanic processes and by extension magma genesis. A feature observed in many Archean greenstone belts but rare in modern volcanic rocks is variolitic texture with millimetre- to centimetre-sized leucocratic globular structures (varioles), in mafic lavas. Models proposed to explain this texture include rapid undercooling, magma mingling and liquid immiscibility.

Here, we investigate samples of Paleoarchean variole-bearing pillow lavas from the ca. 3469 Ma Mount Ada Basalt of the Pilbara Supergroup, Western Australia. The samples contain relict magmatic clinopyroxene and spinel and preserve sharp contacts between varioles and host. No plagioclase is observed in the samples. The clinopyroxene mineral composition is indistinguishable between in the varioles and host. This is despite the variole material having lower MgO and $Fe_2O_3^{(total)}$ and higher SiO_2 and Al_2O_3 concentrations. However, the variole and host materials have indistinguishable TiO_2, Cr_2O_3, NiO_2 and Sm-Nd isotope systematics.

These observations are consistent with an immiscibility reaction from a parental melt to a hydrous fluid phase and conjugate mafic liquid, where minerals that formed before the reaction become incorporated into both endmembers where they continued to grow by diffusive exchange between the hydrous fluid and silicate melt.

Two lines of evidence indicate that hydrous flux exsolution occurred due to H_2O saturation in the precursor magmas, including: (1) the lack of plagioclase, for which crystallisation is supressed at high H_2O content; and (2) Nb/Th < 7, which indicates a hydrated mantle source.

The variole-bearing pillow lavas are part of the 10-Myr-duration Coongan Subgroup volcanic cycle and occur interspersed with tholeiite basalts and minor komatiites of the Mount Ada Basalt and mafic to felsic volcanic rocks of the Duffer Formation. These distinctly different volcanic rock types, which have εNd_i -0.3 ± 0.4, ~1 ε unit lower than contemporary tholeiites, indicate that there was variation in magma genesis, which included hydrous fluxed melting likely genetically related to delamination, during the 10 Myr formation of the Coongan Subgroup volcanic cycle, as part of the Paleoarchean East Pilbara Terrane formation.

Keywords:

Paleoarchean; Pilbara Craton; Variole Texture; Immiscibility; Hydrated mantle source; Magma genesis

1. Introduction

Many Archean greenstone belts contain metabasaltic successions that are characterized by the presence of leucocratic globules, referred to as varioles or ocelli, preserved in lava flows (Ferguson and Currie, 1972; Gélinas et al., 1976; Gélinas et al., 1977; Fowler et al., 1987; Fowler et al., 2002; Komiya et al., 2002; Arndt and Fowler, 2004; Appel et al., 2009; Polat et al., 2009; de Wit et al., 2011; Sandstå et al., 2011; Furnes et al., 2014; Humbert et al., 2018). Variole-bearing metabasaltic lava flows can be volumetrically significant, as documented in the 2.7-km-thick mafic volcanic sequence of the ca. 3470 Ma Hooggenoeg Complex, Barberton Greenstone Belt, South Africa (Sandstå et al., 2011; Furnes et al., 2014), throughout the Nondweni Greenstone Belt, Barberton Greenstone Belt, South Africa (Wilson and Adrian Versfeld, 1994) and in various occurrences throughout the >15 km stratigraphy of the ca. 3530-3220 Ma Pilbara Supergroup of the East Pilbara Terrane, Western Australia (Komiya et al., 2002; Smithies et al., 2007a).

The formation of the variole texture has been variably attributed to i) magma mingling (Fowler et al., 2002; Appel et al., 2009; Krassivskaya et al., 2010), ii) undercooling (Fowler et al., 1987; Fowler et al., 2002; Arndt and Fowler, 2004; Sandstå et al., 2011; Humbert et al., 2018), and iii) immiscibility reactions (Ferguson and Currie, 1972; Gélinas et al., 1976; Gélinas et al., 1977; Gudin et al., 2012). These different mechanisms of variole formation have different petrogenetic implications, making them key indicators of underlying petrogenetic processes with the potential to critically inform models for the formation of early Earth crust.

A magma mingling origin (i) is proposed based on the presence of xenocrystic zircon in varioles from the ca. 3075 Ma Ivisaartoq greenstone belt, SW Greenland (Polat et al., 2002; Appel et al., 2009), where felsic varioles are interpreted to represent partial melts of Eoarchean crust that mingled with younger basaltic magma. In this instance, the variole-bearing lavas have the potential to inform on the nature of the precursor crust upon which greenstone belts formed.

An undercooling origin (ii) for variole textures (Fowler et al., 1987; Fowler et al., 2002; Sandstå et al., 2011; Humbert et al., 2018) suggests eruption of lavas with no mineral load at temperatures significantly above their liquidus due to eruption from depth without significant cooling during transport. Such a mechanism of formation can provide valuable insights into the nature of magma plumbing systems, the prevailing temperatures and melt-generating processes in source regions, and the mode of eruption of the greenstone volcanic piles.

An immiscibility origin (iii) was initially proposed for variolitic lavas from the Barberton greenstone belt, South Africa (Ferguson and Currie, 1972) and from the Abitibi greenstone belt, Canada (Gélinas et al., 1976). More recently, immiscibility was proposed for variole textures in preserved magmas from the Cretaceous Troodos Ophiolite, based on characteristic fluid exsolution textures (Ballhaus et al., 2015). Ballhaus et al. (2015) argued that magma that was H_2O-saturated at depth led to H_2O-supersaturation upon eruption, causing an exsolution of a H_2O-rich low-density phase and a H_2O-poor high-density phase. Therefore, demonstrating that variole-bearing lavas bear petrological and geochemical evidence for high H_2O content in precursor magmas has important implications for hydrous fluxing during magma genesis.

Key to distinguishing the different formation mechanisms for varioles is the observation of preserved magmatic textures (e.g. Fowler et al., 2002; Sandstå et al., 2011; Ballhaus et al., 2015). In the ca. 3530-3220 Ma Pilbara Supergroup of the East Pilbara Terrane (Hickman, 2012), variole-bearing metabasalt lavas are observed in seven of the eight known volcanic cycles (Smithies et al., 2007a). Despite their potential to inform on petrogenetic processes, there has been no previous detailed study of variole-bearing mafic lavas from the Pilbara Supergroup.

In this study, we present examples of representative variole-bearing pillow lavas that preserve relict magmatic mineralogy and volcanic textures from the Paleoarchean Mount Ada Basalt of the Pilbara Supergroup. These samples allow for development of unambiguous arguments for the origin of variole texture based on relict magmatic texture, mineralogy and mineral composition. We further support these arguments with major and trace element data and Sm-Nd isotopic compositions of variole and host separates. Based on these observations we present constraints that must be considered for the petrogenesis of magmas that form variole textures upon eruption and that have implications for magma genesis during the Mount Ada Basalt volcanic event. We then review these implications by placing the variole bearing samples in context of the different magma types identified in the Coongan Group, which is the fourth volcanic cycle in the East Pilbara Terrane and includes the Mount Ada Basalt and the felsic volcanic dominant Duffer Formation.

2. Geological Setting

The studied variole-bearing rocks come from the western Doolena Gap and the south-eastern Warralong greenstone belts of the East Pilbara Terrane, Western Australia (Figure 1). The western part of the east-west-trending Doolena Gap greenstone belt preserves the Mount Ada Basalt as 10- to 100-metre-sized lozenges of little-altered pillow basalt flows (Figure 1b; Williams, 1999; Williams, 2002; Hickman, 2010; Van Kranendonk et al., 2012; Wiemer et al., 2016).

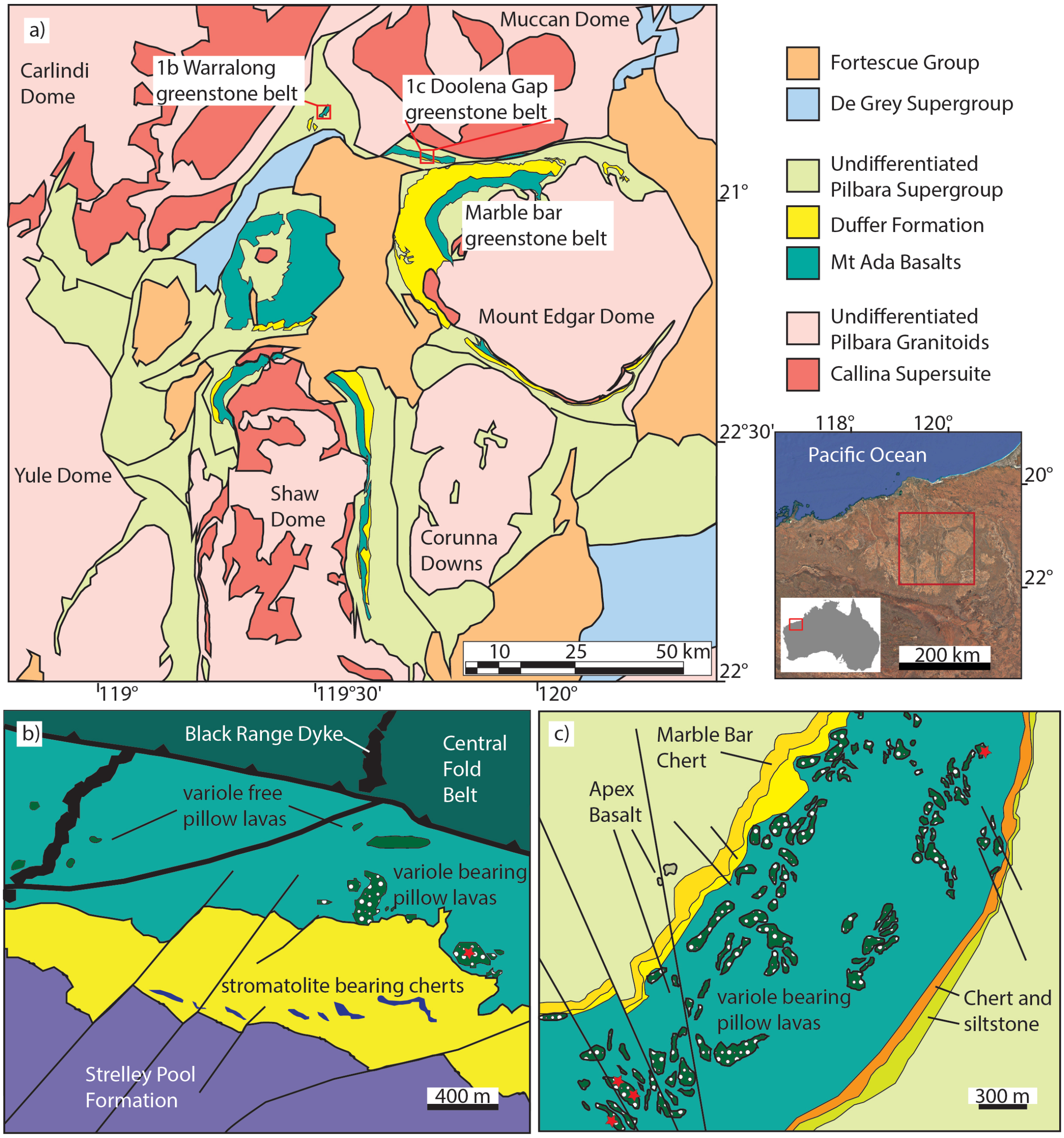

Figure 1: (a) Geological map of the central East Pilbara Terrane showing greenstone belts and granitic complexes modified after Hickman (2012). The spatial extent of the Mount Ada Basalt and the Duffer Formation is shown for greenstone belts in which the Coongan Subgroup outcrops modified after Williams (1999); Williams (2002); Williams and Hickman (2007); Hickman (2010); Van Kranendonk et al. (2012). The spatial extent of the Mount Ada Basalt and the Duffer Formation is shown for greenstone belts in which the Coongan Subgroup outcrops modified after Williams (1999); Williams (2002); Williams and Hickman (2007); Hickman (2010); Van Kranendonk et al. (2012).

Geological map of a sub section of the western Doolena Gap greenstone belt, modified after Wiemer et al. (2016). Outcrops of the Mount Ada Basalt are highlighted in the darker shade of green. The variole-bearing lavas are highlighted with a white stipple and variole free lavas are unpatterned. Studied samples all come from a large lozenge of pillow lavas (red star). (b) Geological map of the Coongan Subgroup in the eastern Warralong greenstone belt highlighting the outcropping Mount Ada Basalt and the location of studied samples (red stars), modified after (Spring, 2017).

Variole-bearing pillow lavas stratigraphically overly variole-free pillow lavas (Figure 1b), which is consistent with the general observation of (Smithies et al., 2007a) that variole-bearing lavas in the East Pilbara Terrane occur at the top of mafic volcanic successions. In the south-eastern portion of the Warralong greenstone belt, the Mount Ada Basalt is preserved as 10- to 100-metre-sized lozenges of little-deformed pillow lavas (Figure 1c). Here, most pillow lavas are variole-bearing and no stratigraphic variation in variole abundance is observed. The pillows range in size from 20 cm to 1.5 m in diameter in both greenstone belts and have little to no vesiculation. Most pillows contain varioles that range in size from 2 to 20 mm. Varioles are rare in pillow margins and abundant in pillow interiors, where they show an increase in size and are often amalgamated (Figure 2). For most pillows the volume of varioles constitutes between 10% and 20% (Spring, 2017).

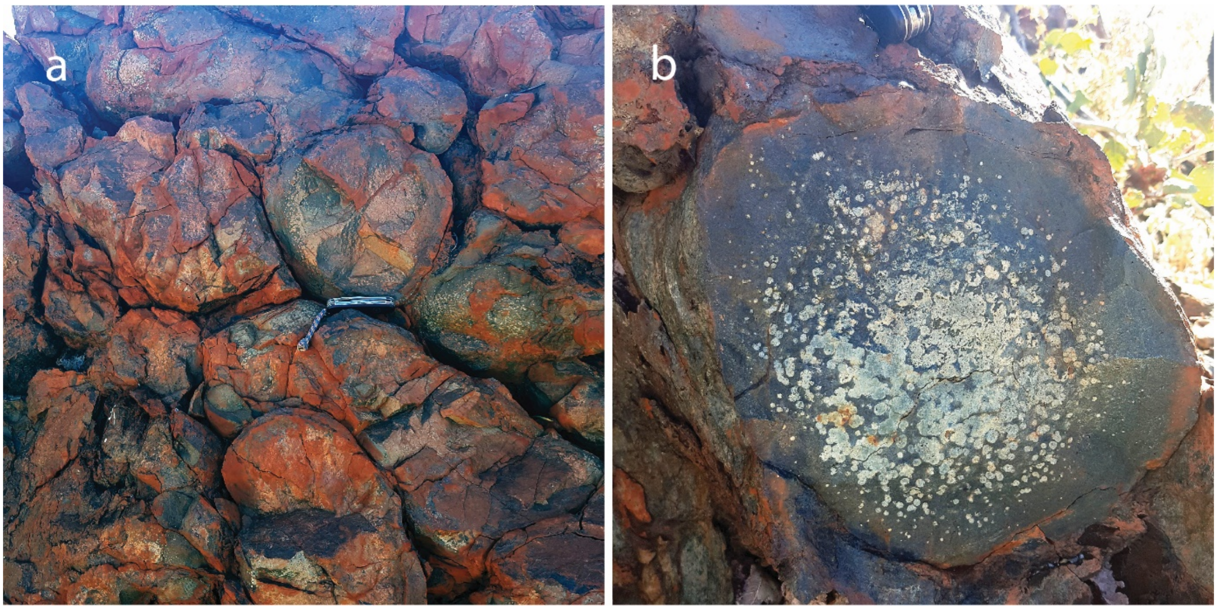

Figure 2: Field images of variole-bearing pillow lavas from the Mount Ada Basalt of the Warralong greenstone belt. (a) shows a stack of pillow lavas that all contain variole texture, (8 cm knife for scale). (b) shows a cross section of a ~10 cm diameter pillow lava tube showing variation in variole texture within the pillow. The pillow margins are almost variole-free. The varioles increase in size towards the pillow interior where they begin to amalgamate.

3. Methodology

Quantitative *in situ* analysis of minerals in thin section, as well as quantitative mapping of individual clinopyroxene crystals were carried out on a field emission electron probe microanalyser (JEOL EPMA JXA-8530F) equipped with five wavelength dispersive spectrometers (WDS) and using Probe Software applications (probesoftware.com). The EPMA spot analysis and WDS stage maps analytical conditions are provided in Supplementary Data 1.

To investigate variation in clinopyroxene composition in the EPMA maps, the map datasets were filtered to preserve only the pixels that yielded stoichiometric clinopyroxene composition according to the following criteria: (1) oxide wt. % totals 98.0 - 102.0, element wt. % Si 21.0 - 26.0, as well as element wt. % Al 0-5.0 and Ca wt. % ≥ 12.0; (2) any remaining pixels registering phosphorous are excluded; (3) mineral formulae for remaining pixels are calculated on the basis of six oxygens per formula unit using the methods and procedures of Deer et al. (2013), with deficiencies in tetrahedral sites (Si) filled to 2 ions per formula unit by Al, and those with Si > 2 ions per formula unit or total cation sums of <3.92 or >4.04 excluded.

For major and trace element analyses, variole-bearing samples were first cut into 2-3-mm-thick slabs. The slabs were sanded to remove residue from the rocks saw. The slab sections were broken into mm-sized fragments, allowing for hand picking of the least altered fragments of purely variole material and the dark coloured host material. One- to three-gram aliquots of each sample were then powdered by hand in an agate mortar and pestle. For the remainder of this paper samples are referred to by their sample ID and whether they represent variole or dark host material. Major element analysis was performed using a WDS XRF PANalytical Axois 1 kW system on fused disks following standard procedures. Due to the small sample size only six samples were analysed for loss on ignition, which was performed on ~10 mg of sample using a Netzsch simultaneous thermal analyser 449 F3. Samples were loaded into the previously heated sintered alumina vials, to ensure stable background for background subtraction, and heated from room temperature to 1100°C with continuous thermo gravimetric analysis. The loss on ignition was calculated as the percentage mass change recorded at 1050°C relative to the initial mass.

Trace element analyses were performed with an Agilent 8800 ICP-MS modified from the methods of Eggins et al. (1997) and Kamber (2009), and Sm–Nd isotopic data were obtained using isotope dilution-TIMS methods with high pressure digestion and spike equilibration. Following chemical extraction of Sm and Nd using Tru-spec and Ln-spec column chemistry, analyses were made using a Triton multi-collector thermal ionisation mass spectrometer. Full analytical procedures are provided in Supplementary Data 2.

4. Results

4.1 Petrology

The striking colour contrast between variole and dark host is obvious in hand specimen (Figure 2) and in thin section (Figure 3 and supplementary figures). In all samples, relict clinopyroxene and spinel occur in similar relative abundance in both variole and dark host (Figure 3 and supplementary figures), although clinopyroxene crystals are commonly more altered in the dark host. Carbonate and chlorite pseudomorphs after olivine occur in both components. The dark hosts comprise an altered groundmass of chlorite with abundant epidote. The varioles have a fine-grained grey massive matrix, possibly including clinozoisite. All samples contain abundant carbonate veins. In the Doolena Gap greenstone belt samples, the clinopyroxene crystals are typically acicular, 10 μm wide and up to 200 μm long. In the Warralong greenstone belt samples clinopyroxene occurs as both equant phenocrysts (50-100 μm), with crystals commonly forming clusters, and finer grained acicular crystals, 10s of μm wide and up to 100 μm long. Spinel crystals are present in all samples ranging in size from 20 to 50 μm in the Warralong samples and up to 200 μm in the Doolena Gap samples (Figure 3 and supplementary figures). Spinel crystals are commonly observed as clusters in pseudomorphs after olivine. Plagioclase or pseudomorphs after plagioclase are not observed in any variolitic sample.

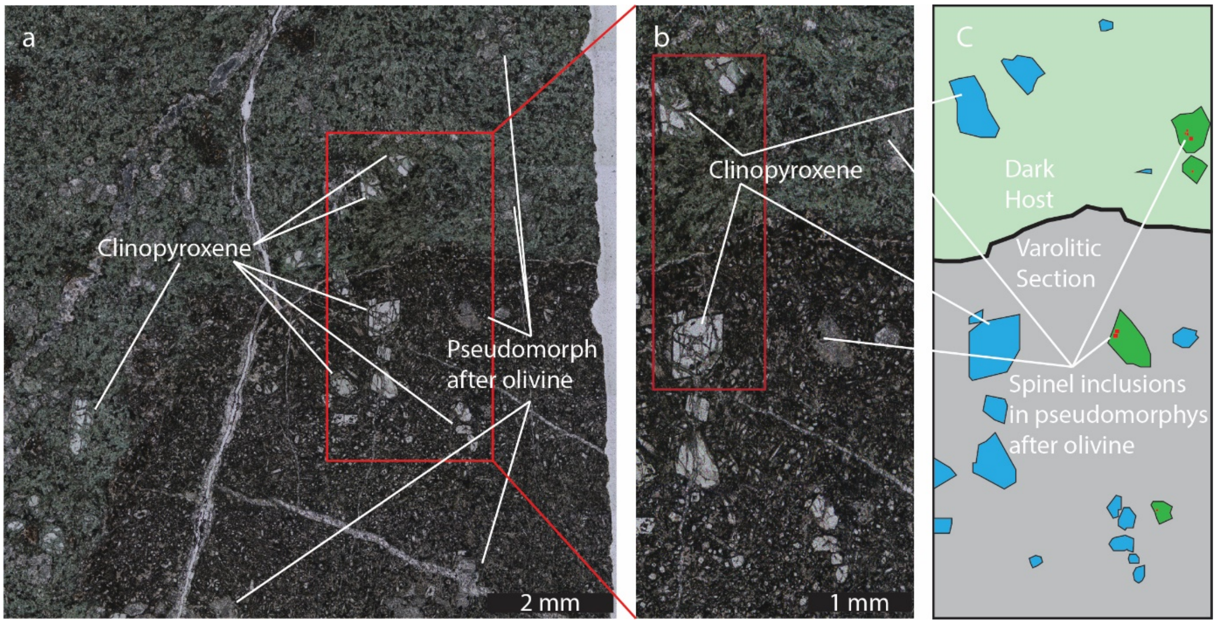

Figure 3: (a) plain polarised light image of Warralong greenstone belt sample JDK-73 showing the sharp boundary between a variole (lower right-hand side) and the host. The full thin section image can be seen in Supplementary Figures. Abundant preserved magmatic clinopyroxene phenocrysts and carbonate pseudomorphs after olivine are present. The sample is cut by fine carbonate veins. The area in the red rectangle is shown in panels b and c. (c) sketch outlining the large clinopyroxene grains, the carbonate pseudomorphs after olivine and the spinel crystals that commonly occur in the carbonate pseudomorphs after olivine. The red rectangle in B shows the location of the EPMA map shown in Figure 5.

4.2 Mineral Composition

Pyroxene compositions are similar both between the two greenstone belts and between variole and dark host in individual samples (Supplementary Electronic Data 1). Based on the spot analyses, each sample displays significant core-rim zonation in larger crystals of both variole and host clinopyroxene as well as overlap in compositional range between variole and host clinopyroxenes. Zoning patterns were explored in greater detail by quantitative maps from each sample (Figure 4), that illuminate complex zoning in some grains, and reveal sharp gradients near crystal rims towards ferroan augite in pyroxenes from both varioles and host material.

Pyroxene crystals from samples from both greenstone belts are enriched in Cr (Cr_2O_3 up to 1.0 wt%; Supplementary Electronic Data 1) where Cr defines oscillatory growth and sector zoning (Figure 4). Large clinopyroxene crystals commonly show zones of chlorite alteration with high Fe (> 13.5 wt. %) that fail the criteria to be clinopyroxene pixels. The Cr zonation can still be seen despite the alteration (Figure 4).

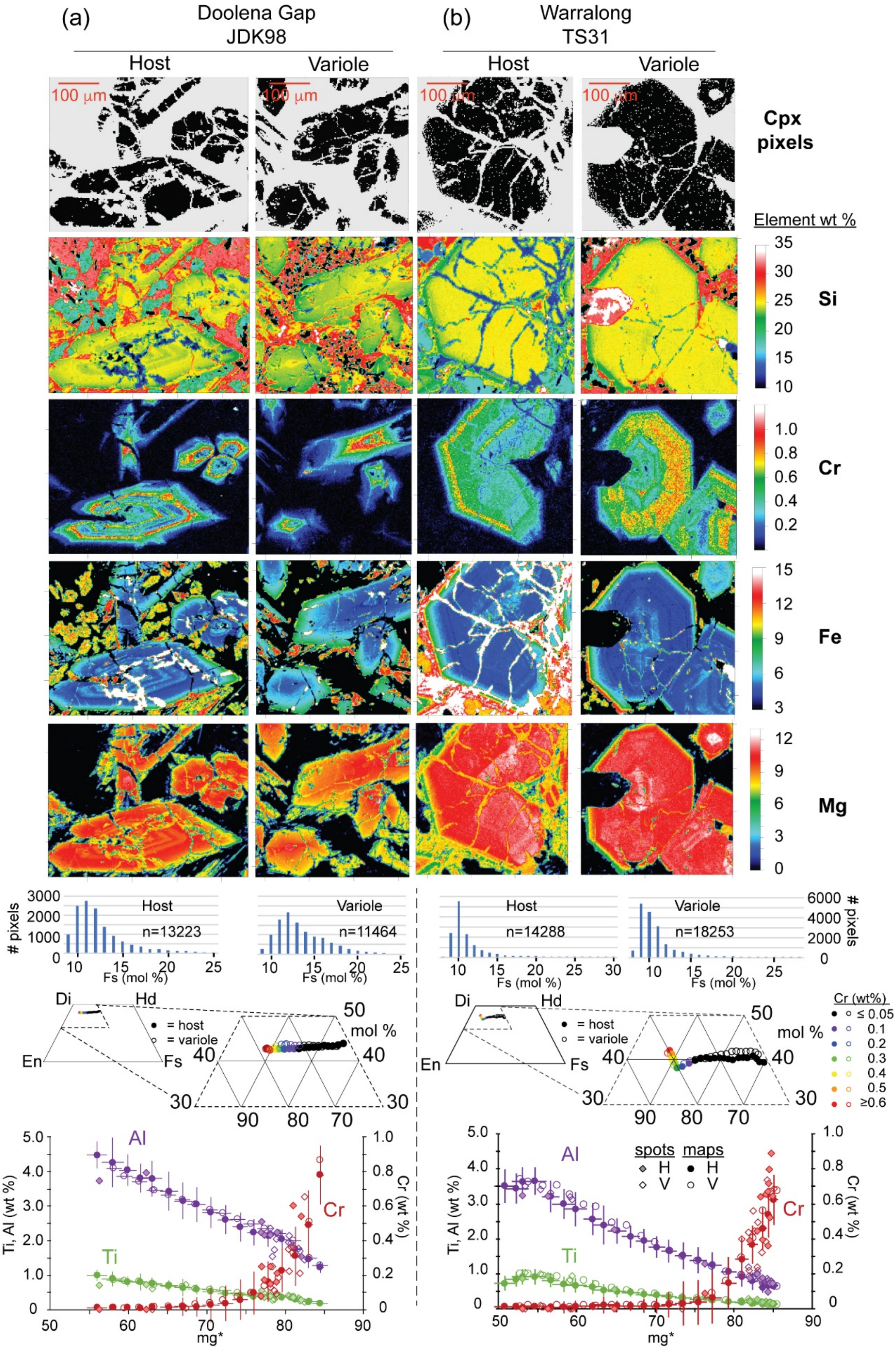

Figure 4. Quantitative EPMA-WDS stage maps comparing clinopyroxenes from varioles and hosts in metabasalts from Doolena Gap and Warralong greenstone belts. The top panel shows

distribution of pixels (in black) that pass filtering criteria for quadrilateral clinopyroxenes (see text). Map rows show element wt % for Si, Cr, Fe and Mg with colour scaled legends at right. Pyroxene quadrilaterals plot medians of pixels binned by increments of 1 % Fs from 5-40%, with host and variole pyroxenes represented by filled and open symbols respectively. Medians are also colour coded according to Cr content (wt%). (a) Representative pyroxenes from Doolena Gap sample (JDK98). The large host pyroxene shows pronounced oscillatory zoning with at least three cycles of enrichment in Cr, and normal zoning (Fe-enrichment) at outermost rims. Oscillatory zoning as well as sector zoning is suggesting in the variole pyroxene. Pyroxene quadrilateral shows close overlap in composition and range shared by variole vs host pyroxene. (b) Warralong sample TS31 also shows very similar behaviour between variole and host pyroxenes, with at least two episodes of Cr enrichment, a distinctive excursion to higher Wo component at Fs ~12 % in both host and variole grains, as well as a shared sharp zonation at outer rims toward ferroaugite.

The pyroxene map datasets were processed further for purposes of statistical comparison between variole versus host pyroxenes. Map datasets were reduced to include only pixels passing the pyroxene filtering criteria defined above. In order that variole and host pyroxenes for the Warralong sample TS31 and the Doolena Gap sample JDK98 could be more aptly compared, this dataset was split to create two small rectangular maps of ~12,000 pixels each that feature the large pyroxenes in the host and variole respectively, and with the variole-host boundary area excluded entirely. Binned statistics were subsequently generated for each variole and host map dataset (including element wt. %) with medians, standard deviations and pixel counts computed for bins of equal size ($Fs_{0.01}$) from $Fs_{0.05}$ to $Fs_{0.40}$ (boundary cases apportioned downward). Total pyroxene pixel counts for each map range from ~12,000 – 40,000. Bin medians for variole and host pyroxenes are plotted for comparison in pyroxene quadrilateral diagrams (Figure 4; those with fewer than 20 pixels are excluded from consideration), that serve to compare trajectories and range of compositional evolution for variole pyroxenes versus those in hosts. Bivariate plots of median element wt. % from the binned map data are plotted together with the single spot EPMA measurements to illustrate consistency of results obtained using the two methods.

In addition, a larger area quantitative EPMA-WDS map shows the variole-host boundary for Warralong greenstone belt sample JDK 73 (Figure 5, Supplementary Figures). This map shows that clinopyroxene in the host is not as well preserved as in the variole. Despite the better preservation of the variole clinopyroxenes, the composition of the pyroxenes is indistinguishable between host and variole.

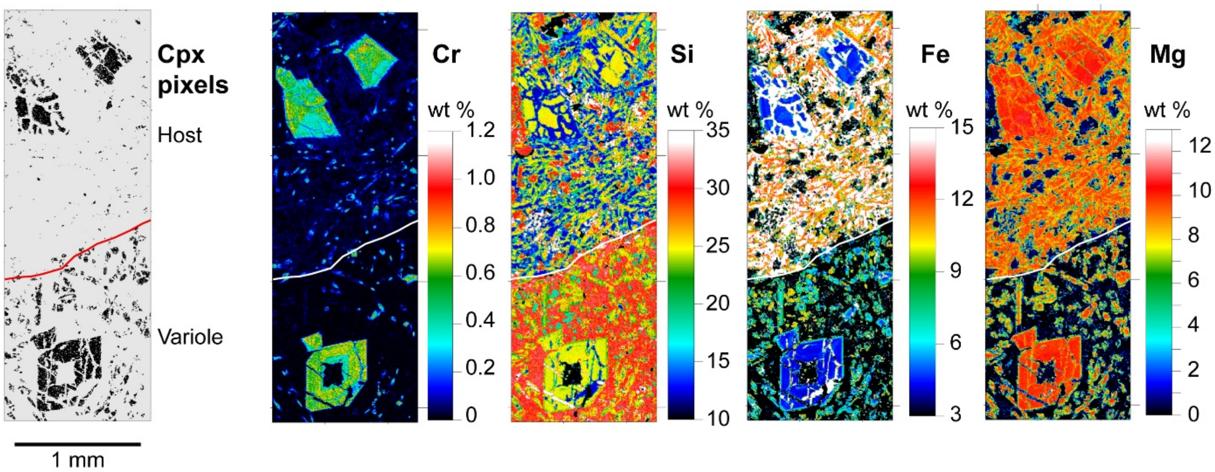

Figure 5. Warralong sample JKD73-2 mapped at larger scale traversing variole-host boundary. The left panel showing pixels defined as clinopyroxene highlights the higher proportion of groundmass pyroxene in the variole section. Elemental maps illustrate sharp contrasts in Si, Fe and Mg in groundmass, whereas pyroxenes are nearly identical in composition in host and variole and preserve similar magmatic zoning patterns.

4.3 Geochemistry

4.3.1 Major and trace element composition

There are significant compositional differences between the bulk compositions of varioles versus dark host separates from samples in both greenstone belts, as summarized in bivariate plots (Figure 6) and illustrated in the quantitative EPMA-WDS map that traverse the boundary between a variole and surrounding host material (Figure 5). The host separates from both greenstone belts have relatively high MgO and $Fe_2O_3^{(total)}$ (Figure 5 and 7).

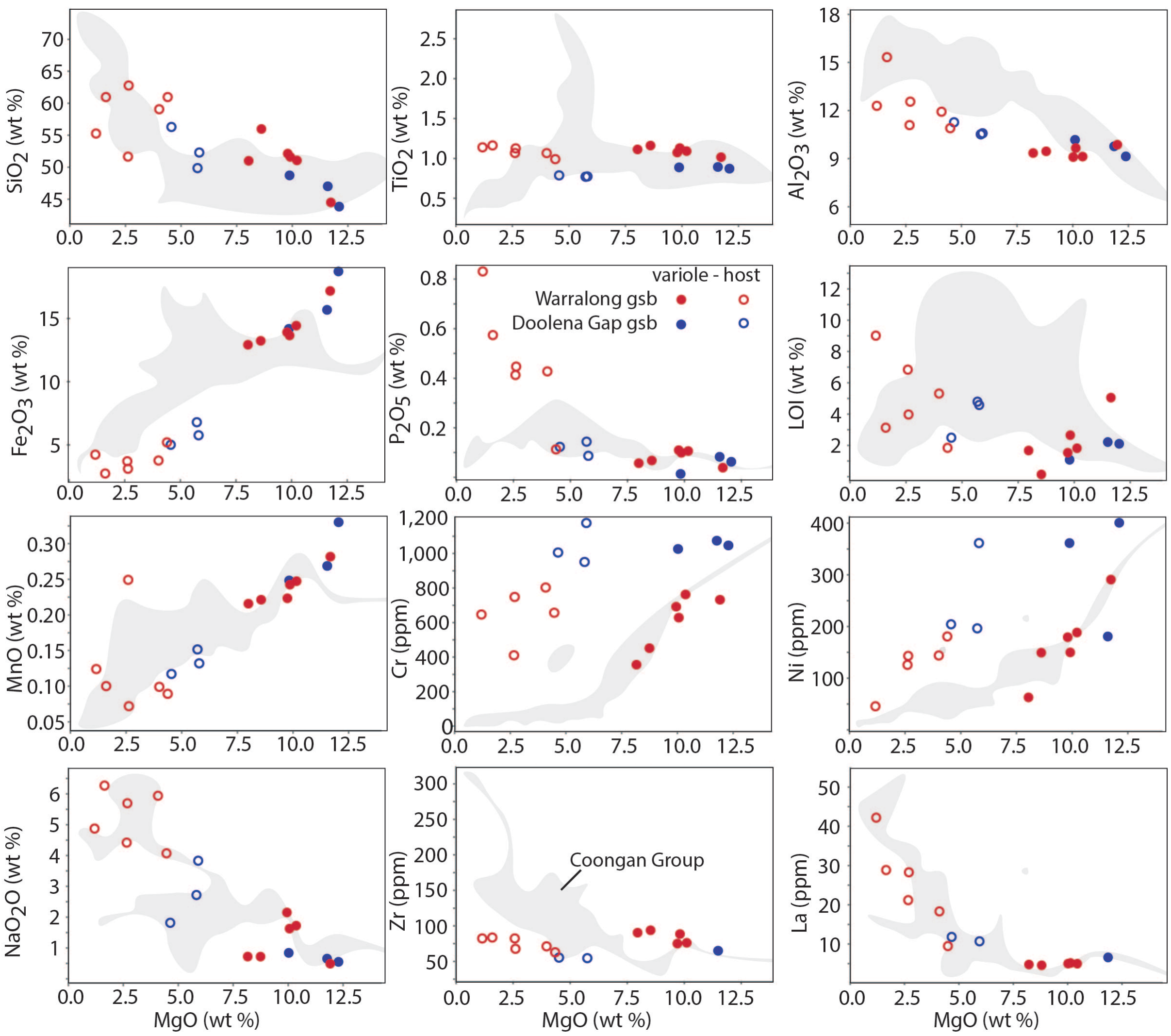

Figure 6: Bivariate plots of select major and trace elements against MgO for variole and dark host of variole-bearing pillow lavas from both the Warralong and Doolena Gap greenstone belts. Also shown are fields for the Coongan Group, that includes the Mount Ada Basalts and Duffer

Formation from Smithies et al. (2005) Gruau et al. (1987), Rizo et al. (2019) and {Tusch, 2021 #113}.

The variole separates have much lower MgO and $Fe_2O_3^{(total)}$ (Figure 5 and 7). Two variole samples from the Warralong greenstone belt have anomalous high P_2O_5 and one has anomalous high MnO. The CaO content of the variole and dark host separates overlap (Figure 6). Both the variole and dark host separates from the Warralong greenstone belt have higher TiO_2 than observed in the Doolena Gap samples (Figure 6).

The bulk rock Cr and Ni concentrations between the variole and dark host separates in each sample from both greenstone belts are indistinguishable (Figure 6). However, in quantitative maps the host appears to have higher Cr (0.1 wt. %) in the groundmass as compared with the groundmass of the variole (<0.05 wt. %; Figure 5). The Doolena Gap greenstone belt samples have substantially higher Cr content than even the most mafic samples reported in the literature for the Mount Ada Basalt (Figure 6). The high Ni concentration in both variole and dark host separates is consistent with the similar abundance of carbonate pseudomorphs after olivine in both separate types that are expected to have high Ni contents inherited from the altered olivine. For elements such as Th, Zr and Hf, the concentrations of the variole and dark host separates are near indistinguishable (Figure 6 and 7). However, the variole separates have systematically higher La concentration as compared to the dark host separates (Figure 6).

The Warralong greenstone belt dark host separates are slightly light REE enriched relative to heavy REE, have a slight negative Eu anomaly and have a slope in a chondrite normalized REE plot (Figure 7). The Doolena Gap dark host separates display steeper REE patterns (Figure 7). All but one of the Warralong greenstone belt variole separates have dramatically higher ΣREE, more pronounced Eu anomalies and steeper chondrite normalised REE pattern than the dark host separates (Figure 7). The REE systematics of the Doolena Gap variole separates either partially overlaps with the dark host separates or have slightly higher ΣREE with notable elevation in La, Ce and Pr (Figure 7).

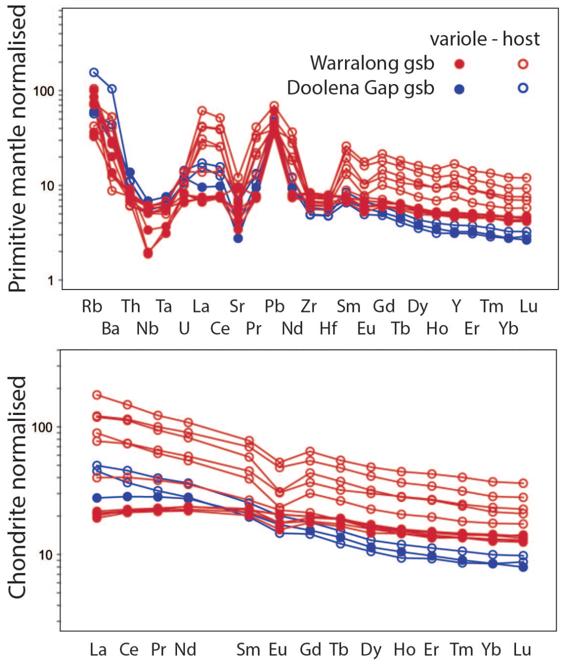

Figure 7: Primitive mantle normalised multi-element spider plots and chondrite normalised plots after Sun and McDonough (1989).

4.3.2 Sm-Nd isotopic compositions

Three dark host separates and two variole separates from both greenstone belts were analysed for Sm-Nd isotope compositions. The Sm-Nd isotope data yield a linear regression that corresponds to an age of 3477 Ma ± 36.4 (Figure 8a), which is within error of the expected age of the 3471-3463 Ma Coongan Subgroup (McNaughton et al., 1993; Nelson, 1999; de Vries et al., 2006), and define an intercept $^{143}Nd/^{144}Nd$ of 0.508117 ± 0.000039 that equates to an εNd at 3469 Ma of -0.3 ± 0.4.

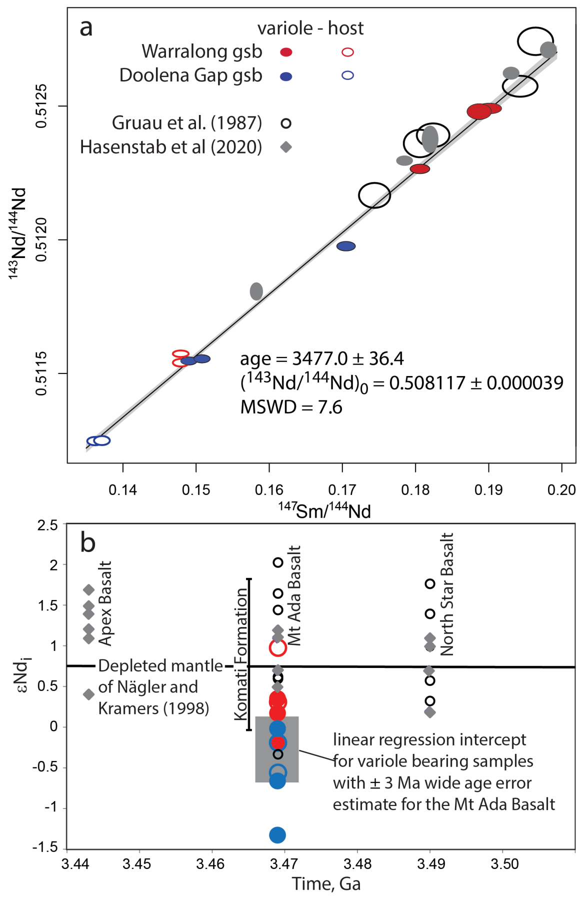

Figure 8: (a) ^{147}Sm/^{144}Nd vs ^{143}Nd/^{144}Nd plot of the Doolena Gap and Warralong greenstone belt variole-bearing samples, with the linear regression generated using IsoplotR of Vermeesch (2018). The Mount Ada Basalt basaltic samples of Gruau et al. (1987) and Hasenstab et al. (2020) are included. (b) Time versus εNd$_i$ at 3469 Ma for the Doolena Gap and Warralong greenstone belt variole-bearing samples and the linear regression intercept with its error from (a) as a grey bar behind the data, the width of which corresponds to the age for the Mount Ada Basalt 3469 ± 3 Ma (Nelson, 1999). Also shown is the depleted mantle evolution of Nägler and Kramers (1998), Warrawoona Group samples of Gruau et al. (1987) and Hasenstab et al. (2020) and the ^{147}Sm/^{144}Nd vs ^{143}Nd/^{144}Nd linear regression intercept for the Komati Formation of Schneider et al. (2019).

For the Warralong greenstone belt separates, ^{147}Sm/^{144}Nd c of the dark host separates is significantly higher (0.181 to 0.189) than the variole separates (both 0.148). Two of the Doolena Gap dark host separates have near identical relatively low ^{147}Sm/^{144}Nd of 0.151 and 0.149 and the third sample has higher $^{147}Sm/^{144}Nd$ of 0.171, whereas the variole separates plot with relatively low $^{147}Sm/^{144}Nd$ of 0.137 and 0.136. The εNd_i (3469 Ma) of Warralong greenstone belt separates have a narrow range from 0.98 to -0.19 with no significant difference between the variole and dark host separates (Figure 8b). The εNd_i (3469 Ma) of Doolena Gap greenstone belt separates range from -0.02 to -1.34, slightly overlapping with the data for the Warralong greenstone belt separates but extending to significantly lower εNd_i (Figure 8b). The εNd_i (3469 Ma) of the linear regression intercept is within error of CHUR and plots with lower εNd_i than estimates of contemporaneous depleted mantle (Nägler and Kramers, 1998).

The separates from variole-bearing lavas have generally lower εNd_i (3470 Ma) than basalt samples of Gruau et al. (1987) and Hasenstab et al. (2020) from the Mount Ada Basalt as well as the 3443 Ma Apex Basalts and 3490 Ma North Star Basalt and the εNd_i at 3465 Ma of the intercept of the linear regression defined by komatiite and basalt samples from the 3465 Ma Komati Formation, Barberton greenstone belt, South Africa (Figure 8b; Schneider et al., 2019).

5. Discussion

In the first part of the discussion (5.1), we concentrate on assessing whether predictions of the various proposed models for the formation of variole texture are consistent with our observations. In the second part (5.2, 5.3) we investigate the petrogenesis of the precursor magma to the variole bearing lavas. In the third part (5.4), we place the precursor magma composition in the context of the temporally and spatially associated volcanic lithologies of the Coongan Group, which includes the Mt Ada Basalt and the Duffer Formation.

5.1 Origin of the Mt Ada Basalt variole texture

Here we investigate the origin of the variole texture by comparing the preserved textures to those predicted for the three models, rapid undercooling, magma mingling and liquid immiscibility proposed for variole formation. We then exclude models based on inconsistencies between predicted and observed textures.

A magma mingling origin between mafic and felsic liquids for variole texture in the pillow lavas in the Doolena Gap and Warralong greenstone belt can be refuted based on the identical clinopyroxene composition between variole and host and the sharp interfaces between variole and host. In modern examples of magma mingling, the mineral load of the two different liquids remain distinctly different (Sparks and Marshall, 1986). Furthermore, magma mingling does not produce sharp interfaces because in mingled systems the mingling liquids are unlikely to be in equilibrium and the interface should show reaction textures. Additionally, magma mingling is not consistent with varioles being concentrated at the centre of pillow lavas.

Likewise, a supercooling origin for the variole can be refuted due to the presence of abundant micro-phenocrysts in both the Doolena Gap and Warralong greenstone belt pillow lavas and the lack of radially arranged plagioclase and/or clinopyroxene in the varioles (Figure 3 and Supplementary Figures). When a magma is emplaced significantly above its liquidus temperature due to eruption from depth without significant cooling during transport, characteristic supercooling textures form because of the paucity of nucleation sites for mineral growth. This results in mineral textures such as dendritic crystals and spherulites (Fowler et al., 2002; Arndt and Fowler, 2004). The presence of phenocrystic clinopyroxene, spinel and pseudomorphs after olivine indicate that the Mount Ada Basalt variole-bearing pillow lavas were not significantly above their liquidus temperatures upon eruption. Furthermore, phenocryst phases are not focal points from which dendritic crystals have grown (Figure 3 and Supplementary Figures).

An immiscibility origin for the variole texture, on the other hand, is consistent with both the sharp boundary between variole and host (Figure 3 and Supplementary Figures) and the identical composition in relict magmatic minerals hosted in both variole and host within the studied samples

(Figures 4 and 5). Sharp boundaries between liquids are expected when they are in equilibrium, as is required for immiscibility reactions (Ballhaus et al., 2015). There are two lines of evidence from the composition of relict magmatic pyroxenes in support of immiscibility. Firstly, the interiors of larger pyroxenes show similar Cr zonation patterns in both variole and host (Figure 4), consistent with magma recharge in a magma chamber prior to eruption, as has been observed in modern volcanic rocks (e.g. Ubide and Kamber, 2018). This indicates that the pyroxene crystals in both variole and host had a common magma history prior to the immiscibility reaction. Secondly, the rims of pyroxene in both variole and host have identical composition. This can be seen most clearly in sample TS31 (Figure 4) where there is a distinct low Mg and high Fe rim to both the variole and host pyroxene crystals that correspond to the near identical data trend for variole and host pyroxenes toward the hedenbergite apex in the pyroxene quadrilateral (Figure 4). It is possible that these pyroxene rims represent pyroxene growth after the immiscibility reaction. If correct, this indicates that the activities of all components were identical, which is a requirement in immiscible systems (Ballhaus et al., 2015).

However, as both the variole and host compositions have silicate matrices, the variole-forming immiscible reaction is not a classic liquid immiscibility reaction in which two liquids with different matrices exsolve from each other, such as in carbonate-silicate immiscible systems (Freestone and Hamilton, 1980; Kjarsgaard and Hamilton, 1988; Kjarsgaard and Peterson, 1991), because silicate liquids are miscible in all proportions. Ballhaus et al. (2015) observed similar silicate-silicate immiscible relationships in the Troodos ophiolite, which they concluded was the result of a fluid phase exsolution from H_2O saturated magmas that erupted in deep water where H_2O degassing was hampered. Ballhaus et al. (2015) argued that the pressure was too low for the hydrous fluid phase to have a high solute load and, therefore, proposed that the initial fluid phase was H_2O dominant. The fluid phase then evolved towards a silicate dominant composition due to preferential incorporation of pre-existing crystals, which continued to grow through solute transfer (e.g. Ca, Si, O) from the conjugate liquid. While this model remains to be tested experimentally, the arguments are the same for the Mount Ada Basalt variole-bearing pillow lavas. Here, we propose that the varioles represent remnants of a segregated, immiscible hydrous fluid phase and the host rock represents the conjugate liquid. In this scenario 1) the original immiscible endmembers were a hydrous fluid and silicate magma, 2) the composition of the variole reflects diffusive exchange between the matrix magma and the exsolved hydrous fluid and 3) the present siliceous composition of the varioles reflects the composition of variole texture at the time the rock froze and subsequent alteration. This indicates that i) the precursor magmas reached H_2O saturation upon eruption, suggesting that the precursor magma had high H_2O content, and ii) the lavas erupted in deep water where H_2O degassing was inefficient (e.g. Ballhaus et al., 2015).

5.2 Magma Petrogenesis: Contamination versus hydrous fluxed melting

For the variole-bearing lavas, an approximation of the composition of the precursor magmas that underwent liquid immiscibility can be reconstructed from the variole and host compositions. We do this instead of bulk analysis of pillows because the pillow lavas are variably altered and crosscut by carbonate veins. As variole abundance varies between ca. 10-20% in the pillow lavas, we reconstitute model precursor magmas as a mixture of 85% host and 15% variole for the samples from the two greenstone belts. The resultant compositions are low-Al_2O_3 komatiitic basalts (Figure 9a). The two simplest models to explain the composition of the precursor magmas of the Mount Ada Basalt variole-bearing lavas are: 1) contamination of a high Cr and Ni magma such as a komatiite or picrite by

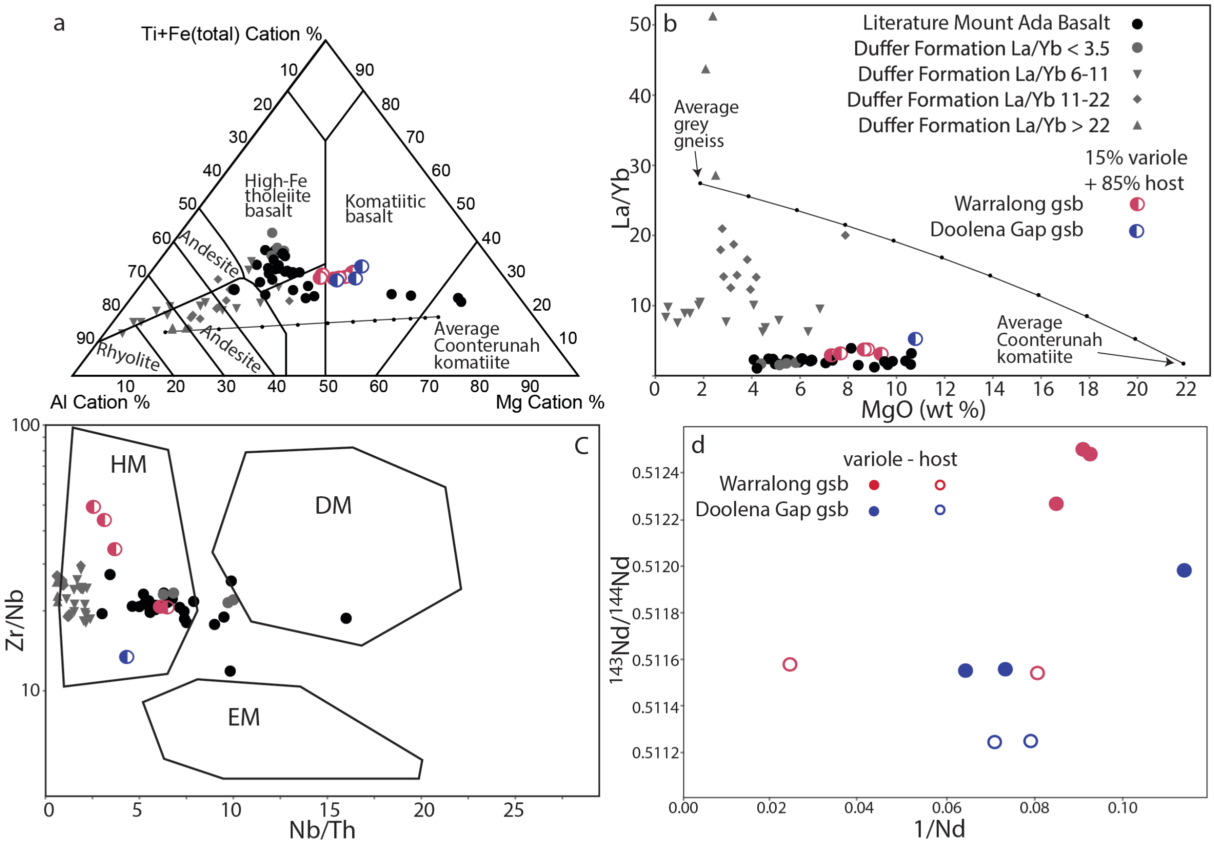

Figure 9: a) Jensen's cation plot after Jensen (1976) and b) MgO versus La/Yb, for the reconstituted model precursor magmas of the Warralong and the Doolena Gap greenstone belt variole-bearing samples together with literature data for the Mount Ada Basalt and the Duffer Formation samples from Gruau et al. (1987), (Smithies et al., 2007a) Rizo et al. (2019) and (Tusch et al., 2021). Also shown is mixing between the average of the Coonterunah komatiites (Smithies et al., 2007a) and average grey gneiss (Moyen and Laurent, 2018). c) plot of 1/Nd vs $^{143}Nd/^{144}Nd$ for the Warralong and the Doolena Gap greenstone belt variole-bearing samples showing a lack of correlation between the samples. d) Zr/Nb vs. Nb/Th discrimination diagram of Condie (2015); HM Hydrated Mantle, DM Depleted Mantle and, EM Enriched Mantle.

material with relatively high La/Yb material such as average grey gneiss (Moyen and Martin, 2012), or 2) the precursor magmas are mantle-derived and formed by hydrous melting of lherzolitic mantle. Here, we use the average komatiite composition from the Coonterunah Subgroup of the Warrawoona Group (Smithies et al., 2005) and the average grey gneiss composition of (Moyen and Martin, 2012) as the most obvious candidates for mixing endmembers. The simplistic bulk mixing model presented in Figure 9a,b clearly cannot replicate the compositions of the precursor magmas of the Mount Ada Basalt variole-bearing lavas. More complex mixing models, where the high La/Yb endmember was a partial melt of average grey gneiss leads to mixing endmembers with higher La/Yb, lower Nb/Th and higher Al relative to Mg and Fe+Ti than the starting composition. Mixing lines between partial melts of average grey gneiss and the Coonterunah komatiites plot further away from the Variole bearing samples than those with average grey gneiss composition as an endmember. Furthermore, the studied samples show no indication of mixing between two components with different Nd isotope compositions based on the plot of 1/Nd vs $^{143}Nd/^{144}Nd$ (Figure 9c). This indicates that there is no evidence pre-existing crust was involved in the petrogenesis of the Doolena Gap or Warralong greenstone belt variole-bearing pillow lavas.

The lack of evidence for crustal contamination, or mixing in general, together with the high water content required for the variole texture to form by hydrous flux exsolution, points towards hydrous fluxed melting as the most likely petrogenetic origin for the variole-bearing pillow lavas. This is consistent with all precursor magmas plotting in the field of hydrated mantle of Condie (2015) (Figure 9d).

5.3 Magma Petrogenesis: Archean volcanic arc versus delamination related volcanism

Hydrous fluxed melting of the upper mantle is typically related to plate tectonics and subduction related dehydration. However, extensive regional scale mapping (Van Kranendonk et al., 2004; Smithies et al., 2005; Van Kranendonk et al., 2006; Van Kranendonk et al., 2007; Van Kranendonk et al., 2015; Nijman et al., 2017) and geochemical investigation of volcanic and plutonic rocks (Smithies et al., 2005; Smithies et al., 2007a; Smithies et al., 2007b; Gardiner et al., 2017) have conclusively demonstrated the lack of arc like processes in the East Pilbara Terrane. Furthermore, Nijman et al. (2017) demonstrated that the basin into which the Mount Ada Basalt was deposited, the Coongan

Basin, was a roughly circular feature and thus not consistent with a quasi-linear morphology expected for an arc setting.

Thus, we propose that a delamination model produced the necessary tectonic conditions for the hydrous fluxed melting. Delamination of hydrated mafic crust into the mantle is a popular model for the origin of Archean tonalite-trondhjemite-granite suites (Johnson et al., 2013; Sizova et al., 2015; Fischer and Gerya, 2016; Nijman et al., 2017; Nebel et al., 2018). The delaminating crust must have undergone dehydration that would lead to a flux of hydrous fluid. If such a hydrous flux permeated through mantle material, melting would occur giving rise to basaltic magma with characteristic geochemical signatures of hydrous fluxed melting, such as low Nb/Th (Figure 9d; Condie, 2015). The relatively low, near chondritic, εNd_i values observed for variole-bearing samples is consistent with this model, because it indicates that there were components in the sources of the precursor magmas that had evolved separately from the contemporary mantle with relatively low Sm/Nd. Here we assume that the contemporary mantle had a εNd_i of +0.75 of Nägler and Kramers (1998), or higher, as is suggested by the average εNd_i of North Star Basalt and Mount Ada Basalt basaltic samples with εNd_i of +1 (Gruau et al., 1987). If the delaminating hydrated mafic crust had evolved for 100 Ma or more, with lower than chondrite Sm/Nd, it could impart a low εNd_i on the basaltic magmas that result from the delamination event. This model can explain the variation in εNd_i between the two greenstone belts where the delaminating hydrated crust was older from the Doolena Gap greenstone belt, average εNd_i of -0.56, compared with the Warralong greenstone belt, average εNd_i of +0.32. This process could also produce the incompatible element enriched basaltic compositions that (Smithies et al., 2009) proposed were necessary to be present in the melt source of early Pilbara granitoids.

Alternatively, the lower εNd_i of the variole containing basalts could represent a separate mantle source. Hasenstab et al, 2021 interpreted Hf-Nd-Ce isotopic systematics of late- early Archean Pilbara mafic and ultramafic rocks as requiring the presence of hybrid mantle sources including upwelling near-chondritic composition mantle as well as Hadean depleted mantle.

5.4 The relationship between the different volcanic geochemical groups in the Coongan Subgroup

Here we place the studied variole bearing pillow lavas in context of the Coongan Subgroup, which represents the third oldest of the eight mafic to felsic volcanic cycles preserved in the Pilbara Supergroup (Hickman, 2012). The Coongan Subgroup includes the basalt dominated Mount Ada Basalt, which includes variole-bearing lavas and rare komatiites (Gruau et al., 1987; Nebel et al., 2014), and the Duffer Formation that contains mafic to rhyolitic volcanic rocks. The geochronological constraints for the Coongan Subgroup were summarised by (de Vries et al., 2006) who concluded that the Coongan Subgroup was deposited over a ten million year time period from 3474 to 3464 Ma. The incompatible trace element pattern for the precursor magmas is subtly different from both non-variole-bearing lavas of the Mount Ada Basalt and samples of the Duffer Formation (Figure 10). The Mount Ada Basalt samples consistently show incompatible element patterns of altered mantle-derived melts, with variable degrees of enrichment and depletion (Figure 7, 10). The Duffer Formation is dominated by samples with high La/Yb and low Nb/Th (Figure 10) and incompatible element patterns similar to average grey gneiss (Moyen and Martin, 2012; Figure 10). The diversity of composition in the Duffer Formation is shown in Figure 10 were we subdivide the unit into 4 components: 1) La/Yb <3.5, 2) La/Yb 6-11, 3) La/Yb 11-22, and 4) La/Yb >22, in agreement with subdivisions of (Smithies et al., 2007a; Smithies et al., 2007b). Importantly, the first three of these groups include basaltic samples (Figure 10b). The precursor magmas have compositions that are transitional between samples with La/Yb <3.5 and Duffer Formation samples with La/Yb >6 (Figure 10c).

That the precursor magmas of the Mount Ada Basalt variole-bearing lavas are chemically transitional between typical mantle-derived magmas and magmas with relatively high La/Yb and low Nb/Th

(Figure 10c) indicates that they record a transition between different magma genesis processes. This is consistent with the observation of (Smithies et al., 2007a) that within the volcanic cycles of the Pilbara Supergroup variole bearing lavas commonly occur at the top of mafic volcanic succession before the transition to felsic dominant volcanics.

The ten million year emplacement period recorded within the Coongan Subgroup (de Vries et al., 2006) is ample time for significant tectonic regime changes to occur that would be required to produce the variations in magma genesis recorded in both the Mount Ada Basalt and the Duffer Formation. We suggest that the proto Pilbara Craton crust was affected by changes in tectonic regimes that are recorded by petrologic and geochemical variations in observed metabasalts.

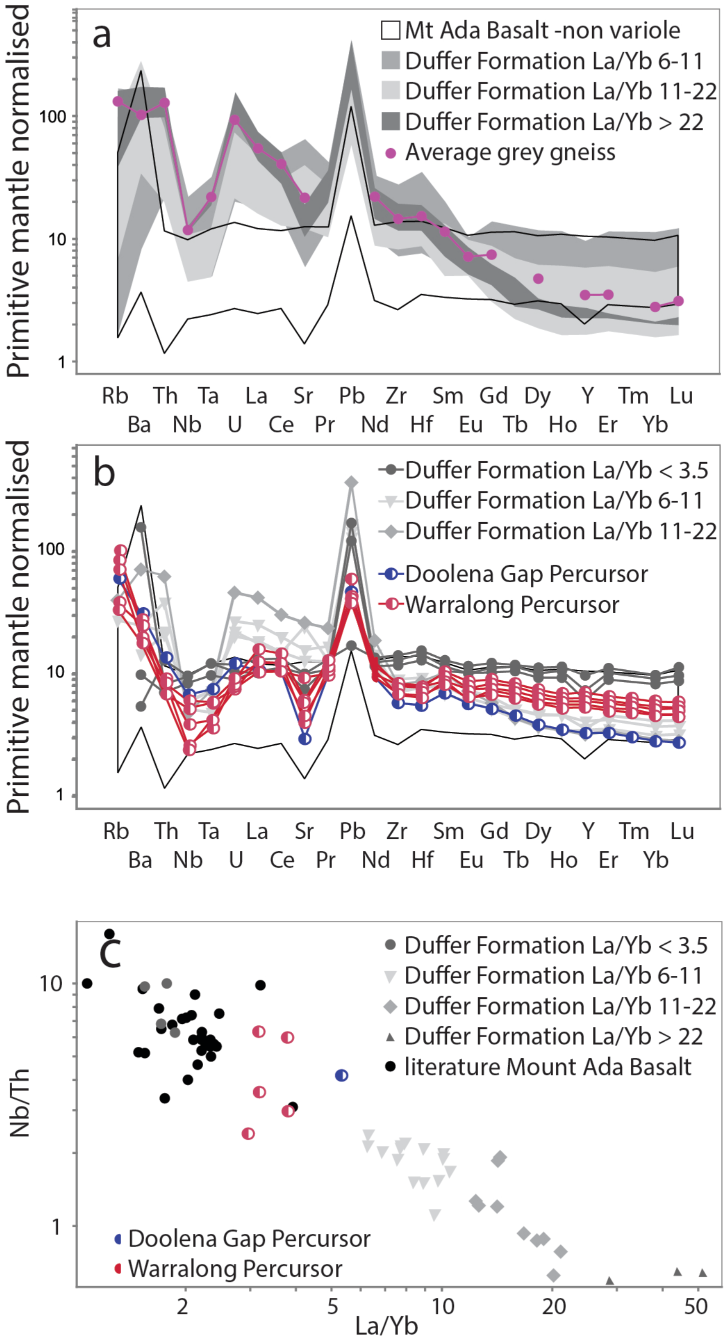

530 Figure 10: Primitive mantle multi-element spider plot normalised after Sun and McDonough (1989) for: a) the Duffer Formation (Smithies et al., 2005) subdivided into three groups; i) La/Yb 6-11, ii) La/Yb 11-22, and iii) La/Yb >22. Duffer Formation samples with La/Yb <2 that are indistinguishable from basalts of the Mount Ada Basalt plot within the Mount Ada Basalt polygon. Also included is the average grey gneiss of Moyen and Martin (2012). b) the precursor magmas of the Warralong and Doolena Gap greenstone belt variole-bearing samples together with the basaltic Duffer Formation

samples. c) plot of La/Yb versus Nb/Th showing that the precursor magmas have an intermediate composition between the non-variole-bearing Mount Ada Basalt samples and the Duffer Formation samples with La/Yb >6 (data from Smithies et al. (2005), Rizo et al. (2019) and Tusch et al. (2021).

6. Conclusions

Detailed textural, mineralogical and chemical observations of samples with preserved primary magmatic mineralogy and texture are essential for deciphering the mechanism of formation of variole textures in basaltic lavas. For the variole-bearing basalts of the Mount Ada Basalt, such evidence indicates that the mechanism of formation of the variole texture was an immiscibility reaction that generated a hydrous flux exsolution and a conjugate silicate liquid. This reaction occurred after the precursor magmas had undergone complex magmatic processes that are recorded in the composition of relict magmatic clinopyroxene. The two liquids underwent diffusive exchange of ions, including Si^{4+}, such that the present silicate composition of the varioles reflects the composition of variole texture at the time the rock froze and subsequent alteration.
relictThe hydrous flux exsolution preserved by the Mount Ada Basalt variole-bearing lavas was the result of H_2O saturation of the precursor magma, as has been proposed for similar textures in the Troodos Ophiolite (Ballhaus et al., 2015). Hydrous fluxed melting of the mantle, likely associated with delamination of hydrated mafic crust, is inferred to be the origin of the high H_2O content of the lavas. The variole-bearing basalts are part of a heterogeneous volcanic magmatic association that formed over the ~10 Ma duration of deposition of the Coongan Subgroup. This includes minor komatiites, low- and high- Ti tholeiiticbasalts, and variole-bearing basalts of the Mount Ada Basalt and the mafic and felsic volcanic rocks of the Duffer Formation, most of which have trace element signatures similar to grey gneiss (Moyen and Martin, 2012). These variations in magma types indicate a diverse and rapidly changing magmatic tectonic environment in the proto-Pilbara Craton crust as recorded in

the ~10 Ma of Coongan Subgroup that has not been considered in existing models for the volcanic cycles in the East Pilbara Terrane. A new generation of models is required that can account for the different magma genesis processes that are required to explain the close temporal and spatial association of komatiites, tholeiites, water saturated mafic lavas (variole bearing lavas) and felsic volcanics.

7. Acknowledgments

Fieldwork campaigns were logistically supported by the Geological Survey of Western Australia. The authors particularly acknowledge the support by A. Hickman (GSWA). Most of the data reported in this paper were obtained at the Central Analytical Research Facility (CARF) Queensland University of Technology. The authors would like to thank Karine Harumi Moromizato and Elizabeth Graham for assistance with CARF analysis. Fieldwork and sampling were undertaken as part of a MSc by Thomas Spring and a PhD by Daniel Wiemer at the Queensland University of Technology. Sm-Nd isotopic analyses at the ANU were supported by ARC Discovery grant DP180100103. We acknowledge the thoughtful and beneficial reviews from Elis Hoffmann and Chris Ballhaus and the handling of the manuscript by Wilson Teixeira.

8. References

Appel, P.W.U., Polat, A., Frei, R., 2009. Dacitic ocelli in mafic lavas, 3.8–3.7 Ga Isua greenstone belt, West Greenland: Geochemical evidence for partial melting of oceanic crust and magma mixing. Chemical Geology, 258(3): 105-124.

Arndt, N., Fowler, A., 2004. Textures in komatiites and variolitic basalts. In: Erikson, K., al (Eds.), The Precambrian Earth: tempos and events. Elsevier, pp. 298-311.

Ballhaus, C., Fonseca, R.O.C., Münker, C., Kirchenbaur, M., Zirner, A., 2015. Spheroidal textures in igneous rocks – Textural consequences of H_2O saturation in basaltic melts. Geochimica et Cosmochimica Acta, 167: 241-252.

Condie, K., 2015. Changing tectonic settings through time: Indiscriminate use of geochemical discriminant diagrams. Precambrian Research, 266: 587-591.

Davis, F.A., Cottrell, E., Birner, S.K., Warren, J.M., Lopez, O.G., 2017. Revisiting the electron microprobe method of spinel-olivine-orthopyroxene oxybarometry applied to spinel peridotites %J American Mineralogist. American Mineralogist, 102(2): 421.

de Vries, S.T., Nijman, W., Wijbrans, J.R., Nelson, D.R., 2006. Stratigraphic continuity and early deformation of the central part of the Coppin Gap Greenstone Belt, Pilbara, Western Australia. Precambrian Research, 147(1): 1-27.

de Wit, M.J., Furnes, H., Robins, B., 2011. Geology and tectonostratigraphy of the Onverwacht Suite, Barberton Greenstone Belt, South Africa. Precambrian Research, 186(1): 1-27.

Deer, W.A., FRS, Howie, R.A., Zussman, J., 2013. An Introduction to the Rock-Forming Minerals. Mineralogical Society of Great Britain and Ireland.

Eggins, S.M. et al., 1997. A simple method for the precise determination of ≥ 40 trace elements in geological samples by ICPMS using enriched isotope internal standardisation. Chemical Geology, 134(4): 311-326.

Ferguson, J., Currie, K.L., 1972. Silicate Immiscibility in the Ancient “Basalts” of the Barberton Mountain Land, Transvaal. Nature Physical Science, 235: 86.

Fischer, R., Gerya, T., 2016. Early Earth plume-lid tectonics: A high-resolution 3D numerical modelling approach. Journal of Geodynamics, 100: 198-214.

Fowler, A.D., Berger, B., Shore, M., Jones, M.I., Ropchan, J., 2002. Supercooled rocks: development and significance of varioles, spherulites, dendrites and spinifex in Archaean volcanic rocks, Abitibi Greenstone belt, Canada. Precambrian Research, 115(1): 311-328.

Fowler, A.D., Jensen, L.S., Pelpquin, S.A., 1987. Varioles in Archean basalts; products of spherulitic crystallization. The Canadian Mineralogist, 25(2): 275-289.

Freestone, I.C., Hamilton, D.L., 1980. The role of liquid immiscibility in the genesis of carbonatites — An experimental study. Contributions to Mineralogy and Petrology, 73(2): 105-117.

Furnes, H., de Wit, M., Dilek, Y., 2014. Precambrian Greenstone Belts Host Different Ophiolite Types. In: Dilek, Y., Furnes, H. (Eds.), Evolution of Archean Crust and Early Life. Springer Netherlands, Dordrecht, pp. 1-22.

Gardiner, N.J. et al., 2017. Processes of crust formation in the early Earth imaged through Hf isotopes from the East Pilbara Terrane. Precambrian Research, 297: 56-76.

Gélinas, L., Brooks, C., Trzcienski Jr, W.E., 1976. Archean variolites—quenched immiscible liquids. Canadian Journal of Earth Sciences, 13(2): 210-230.

Gélinas, L., Trzcienski Jr, W.E., Brooks, C., 1977. Archean variolites and the hypothesis of quench immiscible liquids reexamined: a reply to criticisms. Canadian Journal of Earth Sciences, 14(12): 2945-2958.

Gruau, G. et al., 1987. Age of the Archean Talga-Talga Subgroup, Pilbara Block, Western Australia, and early evolution of the mantle: new SmNd isotopic evidence. Earth and Planetary Science Letters, 85(1): 105-116.

Gudin, A.N., Dubinina, E.O., Nosova, A.A., 2012. Petrogenesis of variolitic lavas of the Onega structure, Central Karelia. Petrology, 20(3): 255-270.
Hasenstab, E. et al., 2020. Evolution of the early to late Archean mantle from Hf-Nd-Ce isotope systematics in basalts and komatiites from the Pilbara Craton. Earth and Planetary Science Letters: 116627.
Hickman, A.H., 2010. Marble Bar, WA 1:250 000 geological sheet SF 50-8. 3rd edition. Geological Survey of Western Australia.
Hickman, A.H., 2012. Review of the Pilbara Craton and Fortescue Basin, Western Australia: Crustal evolution providing environments for early life. Island Arc, 21(1): 1-31.
Humbert, F., Elburg, M.A., Ossa, F.O., de Kock, M.O., Robion, P., 2018. Variolites of the Paleoproterozoic Hekpoort Formation (Transvaal sub-basin, Kaapvaal craton): Multistage undercooling textures? Lithos, 316-317: 48-65.
Jensen, L.S., 1976. A new cation plot for classifying sub-alkaline volcanic rocks. Ontario Division Mines Miscellaneous Paper No. 66.
Johnson, T.E., Brown, M., Kaus, B.J.P., VanTongeren, J.A., 2013. Delamination and recycling of Archaean crust caused by gravitational instabilities. Nature Geoscience, 7: 47.
Kamber, B.S., 2009. Geochemical fingerprinting: 40 years of analytical development and real world applications. Applied Geochemistry, 24(6): 1074-1086.
Kamenetsky, V.S., Crawford, A.J., Meffre, S., 2001. Factors Controlling Chemistry of Magmatic Spinel: an Empirical Study of Associated Olivine, Cr-spinel and Melt Inclusions from Primitive Rocks. Journal of Petrology, 42(4): 655-671.
Kjarsgaard, B., Peterson, T., 1991. Nephelinite-carbonatite liquid immiscibility at Shombole volcano, East Africa: Petrographic and experimental evidence. Mineralogy and Petrology, 43(4): 293-314.
Kjarsgaard, B.A., Hamilton, D.L., 1988. Liquid immiscibility and the origin of alkali-poor carbonatites. Mineralogical Magazine, 52(364): 43-55.
Komiya, T., Maruyama, S., Hirata, T., Yurimoto, H., 2002. Petrology and Geochemistry of MORB and OIB in the Mid-Archean North Pole Region, Pilbara Craton, Western Australia: Implications for the Composition and Temperature of the Upper Mantle at 3.5 Ga. International Geology Review, 44(11): 988-1016.
Krassivskaya, I.S. et al., 2010. Variolitic lavas in the axial rift of the Mid-Atlantic Ridge and their origin (Sierra Leone area, 6°18′N). Petrology, 18(3): 263-277.
McNaughton, N.J., Compston, W., Barley, M.E., 1993. Constraints on the age of the Warrawoona Group, eastern Pilbara Block, Western Australia. Precambrian Research, 60(1): 69-98.
Moyen, J.-F., Laurent, O., 2018. Archaean tectonic systems: A view from igneous rocks. Lithos, 302-303: 99-125.
Moyen, J.-F., Martin, H., 2012. Forty years of TTG research. Lithos, 148: 312-336.
Nägler, T.F., Kramers, J.D., 1998. Nd isotopic evolution of the upper mantle during the Precambrian: models, data and the uncertainty of both. Precambrian Research, 91(3): 233-252.
Nebel, O., Campbell, I.H., Sossi, P.A., Van Kranendonk, M.J., 2014. Hafnium and iron isotopes in early Archean komatiites record a plume-driven convection cycle in the Hadean Earth. Earth and Planetary Science Letters, 397: 111-120.
Nebel, O. et al., 2018. When crust comes of age: on the chemical evolution of Archaean, felsic continental crust by crustal drip tectonics. Philosophical Transactions of the Royal Society A: Mathematical, Physical and Engineering Sciences, 376(2132): 20180103.
Nelson, D.R., 1999. Compilation of geochronological data, 1998. Geological Survey of Western Australia Record 1999.
Nijman, W., Kloppenburg, A., de Vries, S.T., 2017. Archaean basin margin geology and crustal evolution: an East Pilbara traverse. Journal of the Geological Society, 174(6): 1090-1112.
Polat, A., Frei, R., Fryer, B., Appel, P.W.U., 2009. The origin of geochemical trends and Eoarchean (ca. 3700Ma) zircons in Mesoarchean (ca. 3075Ma) ocelli-hosting pillow basalts, Ivisaartoq

greenstone belt, SW Greenland: Evidence for crustal contamination versus crustal recycling. Chemical Geology, 268(3): 248-271.

Polat, A., Hofmann, A.W., Rosing, M.T., 2002. Boninite-like volcanic rocks in the 3.7–3.8 Ga Isua greenstone belt, West Greenland: geochemical evidence for intra-oceanic subduction zone processes in the early Earth. Chemical Geology, 184(3): 231-254.

Rizo, H. et al., 2019. 182W evidence for core-mantle interaction in the source of mantle plumes. Geochemical Perspectives Letters, 11: 6-11.

Sandstå, N.R., Robins, B., Furnes, H., de Wit, M., 2011. The origin of large varioles in flow-banded pillow lava from the Hooggenoeg Complex, Barberton Greenstone Belt, South Africa. Contributions to Mineralogy and Petrology, 162(2): 365-377.

Schneider, K.P. et al., 2019. Petrogenetic evolution of metabasalts and metakomatiites of the lower Onverwacht Group, Barberton Greenstone Belt (South Africa). Chemical Geology, 511: 152-177.

Sizova, E., Gerya, T., Stüwe, K., Brown, M., 2015. Generation of felsic crust in the Archean: A geodynamic modeling perspective. Precambrian Research, 271: 198-224.

Smithies, R., Champion, D.C., Van Kranendonk, M.J., Hickman, A.H., 2007a. Geochemistry of volcanic rocks of the northern Pilbara Craton, Western Australia. Western Australia Geological Survey, Report 104 (2007).

Smithies, R.H., Champion, D.C., Van Kranendonk, M.J., 2007b. Chapter 4.2 The Oldest Well-Preserved Felsic Volcanic Rocks on Earth: Geochemical Clues to the Early Evolution of the Pilbara Supergroup and Implications for the Growth of a Paleoarchean Protocontinent. In: van Kranendonk, M.J., Smithies, R.H., Bennett, V.C. (Eds.), Developments in Precambrian Geology. Elsevier, pp. 339-367.

Smithies, R.H., Champion, D.C., Van Kranendonk, M.J., 2009. Formation of Paleoarchean continental crust through infracrustal melting of enriched basalt. Earth and Planetary Science Letters, 281(3): 298-306.

Smithies, R.H., Van Kranendonk, M.J., Champion, D.C., 2005. It started with a plume – early Archaean basaltic proto-continental crust. Earth and Planetary Science Letters, 238(3): 284-297.

Sparks, R.S.J., Marshall, L.A., 1986. Thermal and mechanical constraints on mixing between mafic and silicic magmas. Journal of Volcanology and Geothermal Research, 29(1): 99-124.

Spring, T.F., 2017. Reconstruction of the physical volcanological processes and petrogenesis of the 3.5Ga Warrawoona Group pillow basalt of the Warralong Greenstone Belt, Pilbara Craton Western Australia. Masters by Research Thesis.

Tusch, J. et al., 2021. Convective isolation of Hadean mantle reservoirs through Archean time. Proceedings of the National Academy of Sciences, 118(2): e2012626118.

Ubide, T., Kamber, B.S., 2018. Volcanic crystals as time capsules of eruption history. Nature Communications, 9(1): 326.

Van Kranendonk, M.J., Collins, W.J., Hickman, A., Pawley, M.J., 2004. Critical tests of vertical vs. horizontal tectonic models for the Archaean East Pilbara Granite–Greenstone Terrane, Pilbara Craton, Western Australia. Precambrian Research, 131(3): 173-211.

Van Kranendonk, M.J. et al., 2006. Revised lithostratigraphy of Archean supracrustal and intrusive rocks in the northern Pilbara Craton, Western Australia. Geological Survey of Western Australia.

Van Kranendonk, M.J., Hugh Smithies, R., Hickman, A.H., Champion, D.C., 2007. Review: secular tectonic evolution of Archean continental crust: interplay between horizontal and vertical processes in the formation of the Pilbara Craton, Australia. 19(1): 1-38.

Van Kranendonk, M.J. et al., 2015. Making it thick: a volcanic plateau origin of Palaeoarchean continental lithosphere of the Pilbara and Kaapvaal cratons. Geological Society, London, Special Publications, 389(1): 83-111.

Van Kranendonk, M.J., Smithies, R.H., Hickman, A.H., 2012. Port Hedland-Bedout Island, Western Australia, 1:250 000 geological sheet SF50-4 and part of sheet SE50-16 - Revised Third edition, Version 1.1. Geological Survey of Western Australia.

Vermeesch, P., 2018. IsoplotR: A free and open toolbox for geochronology. Geoscience Frontiers, 9(5): 1479-1493.

Wiemer, D., Schrank, C.E., Murphy, D.T., Hickman, A.H., 2016. Lithostratigraphy and structure of the early Archaean Doolena Gap greenstone belt, East Pilbara Terrane, Western Australia. Precambrian Research, 282: 121-138.

Williams, I.R., 1999. Geology of the Muccan 1:100000 sheet. . Geological Survey of Western Australia, 1:100000 Geological Series Explanatory Notes.

Williams, I.R., 2002. Yarrie, Western Australia, 1:250 000 geologcal sheet SF 51-1 International Index - Third edition. Geological Survey of Western Australia.

Williams, I.R., Hickman, A.H., 2007. Nullagine, Western Australia, Sheet SF5105, 3rd edition. 1:250 000 Geological Series. Geological Survey of Western Australia.

Wilson, A.H., Adrian Versfeld, J., 1994. The early Archaean nondweni greenstone belt, southern Kaapvaal Craton, South Africa, Part II. Characteristics of the volcanic rocks and constraints on magma genesis. Precambrian Research, 67(3): 277-320.